Green Chemistry

PAPER

View Article Online
View Journal | View Issue

Cite this: *Green Chem.*, 2025, **27**, 4308

P–N synergy with lignocellulosic biomimetic flame-retardant aerogels for effective fire-safe and thermal insulation†

Tao Gui,[a] Shuang-Lin Zou,[a] Hao-Zhen Dou,[b] Wen-Feng Ren,[a] Chang-You Shao,[a] Chun-Lin Xu,[c] Ling-Ping Xiao *[a] and Run-Cang Sun[a]

Received 2nd January 2025,
Accepted 17th March 2025

DOI: 10.1039/d5gc00021a

rsc.li/greenchem

Traditional petroleum-based foams, such as polyurethane and expanded polystyrene, are widely used due to their light weight nature and low thermal conductivity. However, their high flammability and significant environmental impact remain critical challenges. Developing green and sustainable insulation materials from lignocellulose has therefore become a pressing need. In this study, phosphorylated lignin was synthesized using a simple, solvent-free mechanochemical method. Polydopamine (PDA), known for its nitrogen- and catechol-rich composition, was introduced to establish a phosphorus–nitrogen (P–N) synergistic flame-retardant system. This innovation led to the creation of a biomass-based thermal insulation material with excellent fire resistance and heat insulation properties. The composite aerogels demonstrated remarkable performance under high-temperature conditions, forming a robust and stable carbon layer due to synergistic flame-retardant effects. Notably, the fabricated aerogel achieved a limiting oxygen index (LOI) of 35.6% and reduced heat release by over 50%. Additionally, the aerogels exhibited outstanding properties, including superior thermal insulation, effective fire protection, and exceptional UV resistance. These attributes make the material a promising solution for demanding environments, offering a novel approach for the development of next-generation fire-resistant insulation materials.

Green foundation

1. We report a bio-based P–N synergistic flame retardant system for the preparation of flame retardant aerogels. The system is mechanochemically modified to fabricate phosphorylated lignin and simultaneously composite with dopamine surface-modified lignocellulose.
2. Taking advantage of the flame retardant system of the P–N composite system in the gas phase and condensed phase, the aerogel condensed phase exhibits effective charring capacity and a strong dilution effect of heat and combustible gas in the gas phase when exposed to a heat flow.
3. We are committed to designing P–N synergistic flame retardant composite aerogels with excellent comprehensive performance to make greener contributions in the field of engineering flame retardant thermal insulation materials.

1. Introduction

With the rapid advancement of industrial technology, energy consumption has become an increasingly critical issue. In the construction industry, energy usage associated with building insulation materials accounts for a substantial proportion, approximately 40%.[1–4] Petroleum-based foams, including polyurethane (PU), expanded polystyrene (EPS), and phenolic foam board, are commonly utilized as thermal insulation materials in industrial and commercial applications due to their light weight properties and excellent thermal insulation performance.[5–7] Unfortunately, although they offer numerous advantages, the high flammability of the organic polymer matrix imposes significant limitations on industrial applications, leading to fires that continue to inflict immeasurable losses on human life and property each year.[8,9] Furthermore, the use of petroleum-based insulation panels causes significant environmental pollution and sustainability challenges. The non-degradability of foams derived from petroleum-based raw materials has exacerbated the energy and environmental crises, while the pollution caused by waste polymer plastics has emerged as a widely recognized social

[a]*Liaoning Key Lab of Lignocellulose Chemistry and BioMaterials, Liaoning Collaborative Innovation Center for Lignocellulosic Biorefinery, College of Light Industry and Chemical Engineering, Dalian Polytechnic University, Dalian 116034, China. E-mail: lpxiao@dlpu.edu.cn*
[b]*Power Battery and Systems Research Center, State Key Laboratory of Catalysis, Dalian Institute of Chemical Physics, Chinese Academy of Sciences, Dalian 116023, China*
[c]*Laboratory of Natural Materials Technology, Faculty of Science and Engineering, Åbo Akademi University, Henrikinkatu 2, Turku FI-20500, Finland*
† Electronic supplementary information (ESI) available. See DOI: https://doi.org/10.1039/d5gc00021a

issue.[10–12] Consequently, there is an urgent need to utilize biomass energy for the development of new green and safe thermal insulation materials.

Aerogel is a type of material characterized by low density and high porosity, demonstrating significant application potential in the field of thermal insulation materials.[13–16] Furthermore, aerogels fabricated from biomass energy could fundamentally address the environmental pollution issues associated with petroleum-based foams due to their inherent advantages, including ecological friendliness, economic benefits, and biodegradability.[4,17–19] In recent years, numerous researchers have developed a range of biomass composite aerogels utilizing biomass raw materials, including cellulose,[20,21] chitin,[22] gelatin,[23] *etc*. Leveraging the advantages of bio-polymerization, bio-based composite aerogels with high mechanical strength and low thermal conductivity were designed and fabricated. However, akin to traditional petroleum-based insulation foam sheets, most bio-based aerogels also pose potential fire hazards.[24–26]

A simple and effective approach for improving the flame retardancy of polymer materials involves incorporating them as flame-retardant units into polymer molecular chains or physically blending the materials with flame retardants.[27,28] Lignin contains active sites along its macromolecular chain, including phenolic and aliphatic hydroxyl groups.[29,30] Consequently, it is amenable for various chemical modifications, such as functionalization and grafting of flame-retardant segments.[31] More importantly, to achieve high performance of lignin-derived flame retardants with enhanced flame-retardant efficiency, phosphorus (P) and/or nitrogen (N) are typically introduced into the molecular structure through chemical methods.[32,33] For example, Yu *et al.* used lignin as a functional additive for wood–plastic composites (WPC) by chemically grafting phosphorus, nitrogen and copper elements. It not only reduced the heat release rate, but also decreased the total smoke production rate during combustion.[34] Phosphorus-functionalized lignin generally exhibits enhanced flame retardancy in polymeric materials due to its ability to combine the flame-retardant effects of P in both the gas and condensed phases with the carbonization effects of lignin in the condensed phase.[35–37]

In this work, phosphorylated lignin (PL) was fabricated using a solvent-free mechanochemical method. Lignocellulose coated with dopamine (PDA@LCF) was introduced into the system to create a phosphorus–nitrogen (P–N) synergistic flame-retardant system. Furthermore, green and renewable sodium alginate (SA) served as a gel matrix for preparing a composite aerogel material, which showed exceptional fire resistance and thermal insulation properties. More importantly, owing to the synergistic effect of the two components, sodium alginate and the lignocellulosic matrix formed a solid carbon layer through catalytic carbonization, which functioned as a fire barrier.[38,39] The catechyl self-crosslinking of the PDA coating was promoted by the hot acidic environment generated by the PL at high temperatures. This process contributed to the formation of a solid carbon layer with a cohesive structure within the material matrix. Additionally, the phosphoric acid groups in lignin revealed strong free radical scavenging effects, effectively capturing combustion free radicals at the interface to achieve a synergistic flame-retardant effect. Due to this unique synergistic interaction, the fabricated lignin composite aerogel was nearly non-flammable, achieving a limiting oxygen index (LOI) as high as 35.6%. Furthermore, the aerogel exhibited excellent thermal insulation properties, positioning it as a viable alternative to conventional thermal insulation boards. In summary, this work presents an innovative design concept for the development of next-generation fireproof insulation materials. These materials can serve as effective fire protection solutions across a variety of substrates, offering significant application potential in construction, commercial insulation, and related fields.

2. Results and discussion

2.1 Fabrication of phosphorylated lignin

Organophosphorus flame retardants exhibit high flame-retardant efficiency, benefiting from the interruption of the combustion process in the gas phase by releasing PO free radicals.[40,41] Therefore, we employed a solvent-free mechanochemical method to phosphorylate the hydroxyl groups of lignin (Fig. 1a), enhancing the gas-phase free radical capture efficiency of lignin at the combustion interface and thereby improving the flame-retardant properties of the material. Fourier Transform Infrared Spectroscopy (FT-IR) and X-ray photoelectron spectroscopy (XPS) were used to study the lignin samples before and after modification, confirming the successful modification of lignin (Fig. 1b and c). Notably, the FT-IR spectra of L and PL exhibited characteristic peaks of G/S-type lignin.[42] New peaks of P═O and P–O–H/P–O–C were observed at 1013 and 961 cm^{-1}, respectively (Fig. 1b), and the details of the spectrum are presented in Fig. S3 and Table S1.† In addition, the survey spectrum of XPS demonstrated that PL exhibited a P2p peak signal, which also indicated that lignin was successfully introduced with P species (Fig. 1c). Meanwhile, the O1s spectra of L and PL (Fig. S1b†) could be deconvolved into two peaks of C═O (533.0 ± 0.2 eV) and C–O (531.3 ± 0.4 eV). Interestingly, all the peaks of PL were slightly shifted, and the peaks of C–O were somewhat enhanced. This is attributed to the introduction of the P element by way of covalence (C–O–P),[43] which was consistent with that of the P2p spectrum (Fig. S2†).

Furthermore, 2D ^{1}H–^{13}P HMBC NMR was used to characterize phosphorylated lignin and further confirmed the phosphorylation of lignin (Fig. 2). The coupling signals between the phosphate group and the neighboring proton were observed, which suggested that the phosphorus peak (−0.84 ppm) was associated with the two protons of the aliphatic side chain (−3.52 and −3.49 ppm).[44,45] This is attributed to the P–O–R′ signal, where R′ represents the aryl group of lignin. This further indicated that lignin was successfully phosphorylated with the phosphate group primarily attached to the phenolic

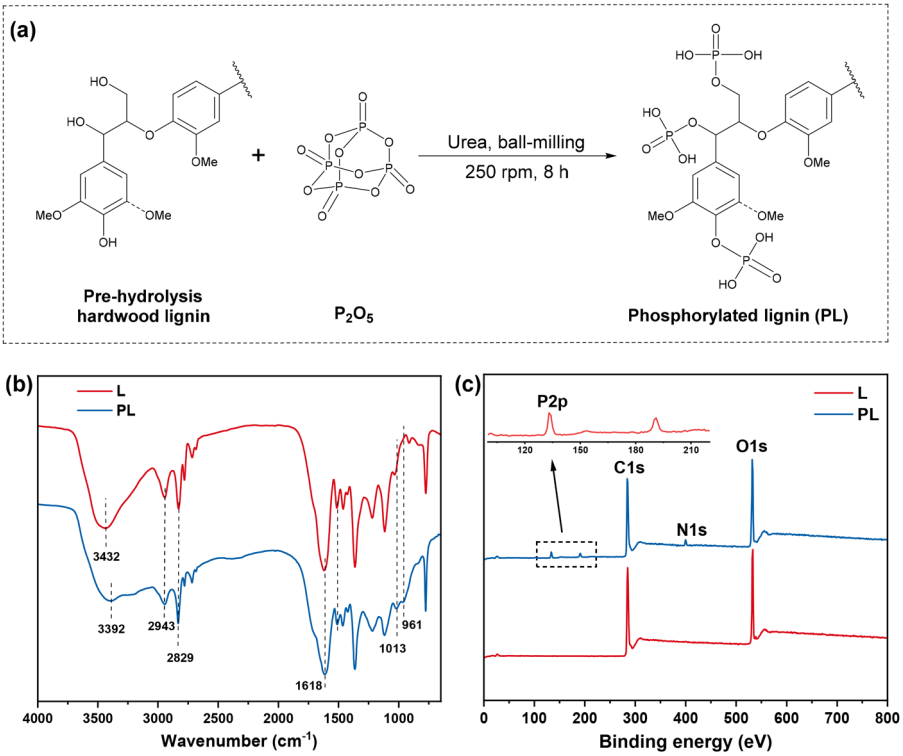

Fig. 1 Phosphorylation process and characterization of lignin. (a) Phosphorylation of lignin. (b) FT-IR spectra of L and PL samples. (c) XPS survey of L and PL.

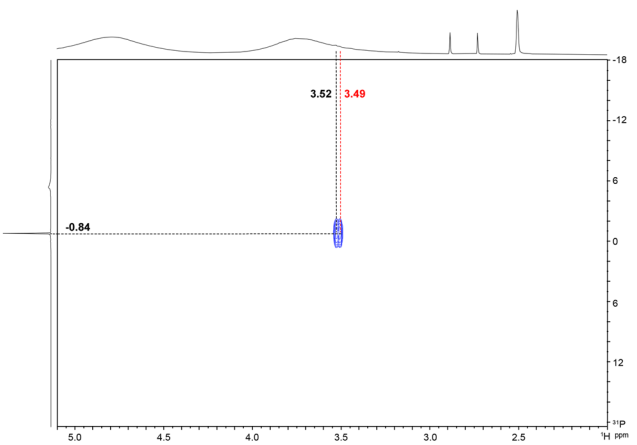

Fig. 2 2D $^{1}H-^{31}P$ HMBC spectrum of phosphorylated lignin (PL).

and fatty hydroxyl groups. Additionally, thermogravimetric analysis (TGA) was performed to reveal the thermal stability of L and PL (Fig. S4†). The initial decomposition temperature of PL was lower than that of L, and showed a higher content of carbon residue. At the early stages of pyrolysis, this is due to the fact that phosphoric acid, generated during the earlier decomposition of PL, accelerated the breakdown of lignin and facilitated its coking process (Fig. S4a†). It is noteworthy that the DTG curve (Fig. S4b†) of PL exhibits multiple distinct peaks and shoulder peaks below the maximum decomposition temperature (T_{max}). Specifically, the peak at 64.5 °C for both PL and L is ascribed to the evaporation of trace water from the material matrix. The shoulder peak observed at 193.2 °C is due the decomposition of the phosphate component in PL molecules, which facilitated the breakdown of lignin. The appearance of a third peak at 278.4 °C indicated that PL had gradually charred and displayed a decreased decomposition rate. As the temperature rose to 379.1 °C, the maximum pyrolysis temperature was reached, which was 20.2 °C lower than that of L, and the pyrolysis rate decreased by 0.19%/°C. These results demonstrated that the phosphoric acid component of PL effectively promoted the carbonization process of lignin and improved its thermal stability.

2.2 Fabrication of the lignin composite aerogel

In general, the incorporation of phosphorus (P) and nitrogen (N) external flame retardants into a material represents an effective approach for achieving high flame retardancy. This was attributed to the inherent synergy of the P–N flame retardant system, which effectively enhanced the flame-retardant performance of the material. Furthermore, phosphorus and nitrogen are currently regarded as the two most environmentally friendly flame-retardant elements. Therefore, we employed PL, containing phosphate groups, and PDA@LCF, which was rich in nitrogen, as external flame retardants for incorporation into the sodium alginate matrix for the preparation of aerogel insulation materials with excellent flame

retardancy. The schematic diagram illustrating the preparation process and the resulting composite aerogel samples are illustrated in Fig. 3a and b, respectively. As anticipated, the fabricated lignin composite aerogel exhibited a vertically oriented microstructure. This anisotropic cell wall structure enhanced the thermal insulation capacity of the material when laterally utilized (Fig. 3c). Additionally, thermogravimetric analysis (TGA) was conducted to evaluate the thermal degradation behavior of the aerogel (Fig. S5†), and detailed data are summarized in Table S2.† Specifically, the samples without PL exhibited poor thermal stability with the maximum degradation rate occurring at approximately 305 °C, where the carbon residue was around 45%. However, the thermal stability of the composite aerogel was notably improved with the addition of PL. It is important to highlight that as the PL content increased, the thermal stability of the composite also gradually enhanced. Upon reaching a decomposition temperature of 800 °C, the carbon residue of the 40 wt% lignin composites was observed to be as high as 56%. More importantly, with the increase in PL content, its DTG peak distribution shifted (Fig. S5b†). Following the addition of lignin, the initial decomposition temperature (T_i) was elevated to 256 °C, and a corresponding shift in the peak maximum decomposition temperature (T_{max}) was also observed. Among them, the T_{max} of 40% lignin composite was 326 °C, which was 77 °C higher than that of pure SA. Accordingly, it could be concluded that single PDA@LCF cannot improve the material thermal stability. Upon incorporating a high concentration of phosphorylated lignin (PL) into the system, synergistic interactions between the phosphate groups of PL and the nitrogen-rich PDA@LCF significantly enhanced the material's coke-forming ability, thereby improving its thermal stability.

2.3 Fire-safe performance and mechanism

Notably, one of the most important properties of thermal insulation foam is fire prevention performance.[46,47] Herein, the flame retardancy of composite aerogel were tested by limiting oxygen index (LOI) and vertical combustion test, and the results are displayed in Fig. 4. To evaluate the flame-retardant properties of lignin composite aerogel, the vertical combustion tests were performed for 20s (Fig. 4a, b, and S6†). Notably, the flame retardancy of the PDA@LCF sample was poor due to its singular nitrogen source and the absence of essential flame-retardant components. To enhance the flame retardancy of the material, PL was utilized as the primary flame retardant with its content controlled at 10 ~ 40 wt%. Furthermore, a vertical combustion test was conducted on varying lignin contents (Fig. 4b). The detailed photograph and movies of combustion tests of the 40 wt% PL sample are depicted in Fig. S6 and Movie S1,† respectively. The results indicated that varying degrees of flame retardancy exhibited as the content of PL increased. The flame retardancy was relatively poor at lower PL contents of 10 wt% and 20 wt%. However, when the lignin content was increased to 30 wt%, the flame retardancy of the composite aerogel improved, with the optimal flame-retardant effect observed at a PL content of 40 wt%. Additionally, commercial insulation materials, namely polystyrene (PS) and polyurethane (PU) were purchased for direct combustion comparison (Movies S2 and S3†). The results indicated that both PU and PS generated significant amounts of black smoke during combustion and exhibited a faster combustion rate. Furthermore, the findings demonstrated that the flame retardancy of the PL composite aerogel surpassed those of the above materials.

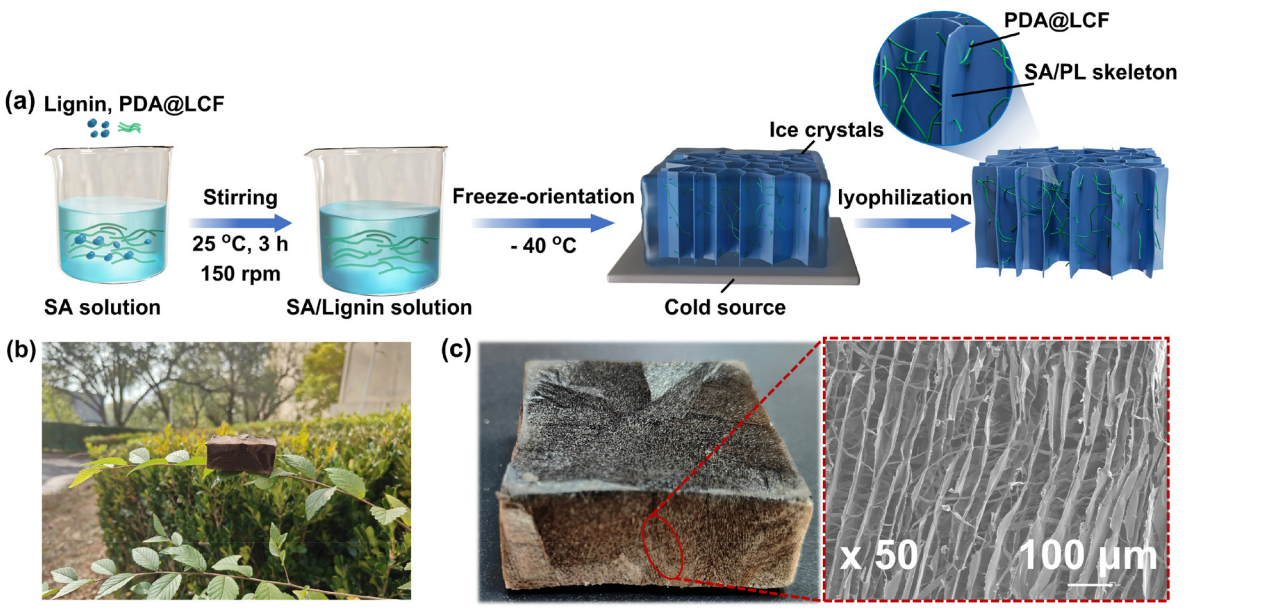

Fig. 3 (a) The scheme of lignin composite aerogel prepared by using PDA@LCF and PL as flame-retardant components. (b) An optical image displaying the PDA@LCF/SA-PL40 aerogel resting on the leaves of a plant. (c) optical image of the PDA@LCF/SA-PL40 aerogel and SEM image of the cross section.

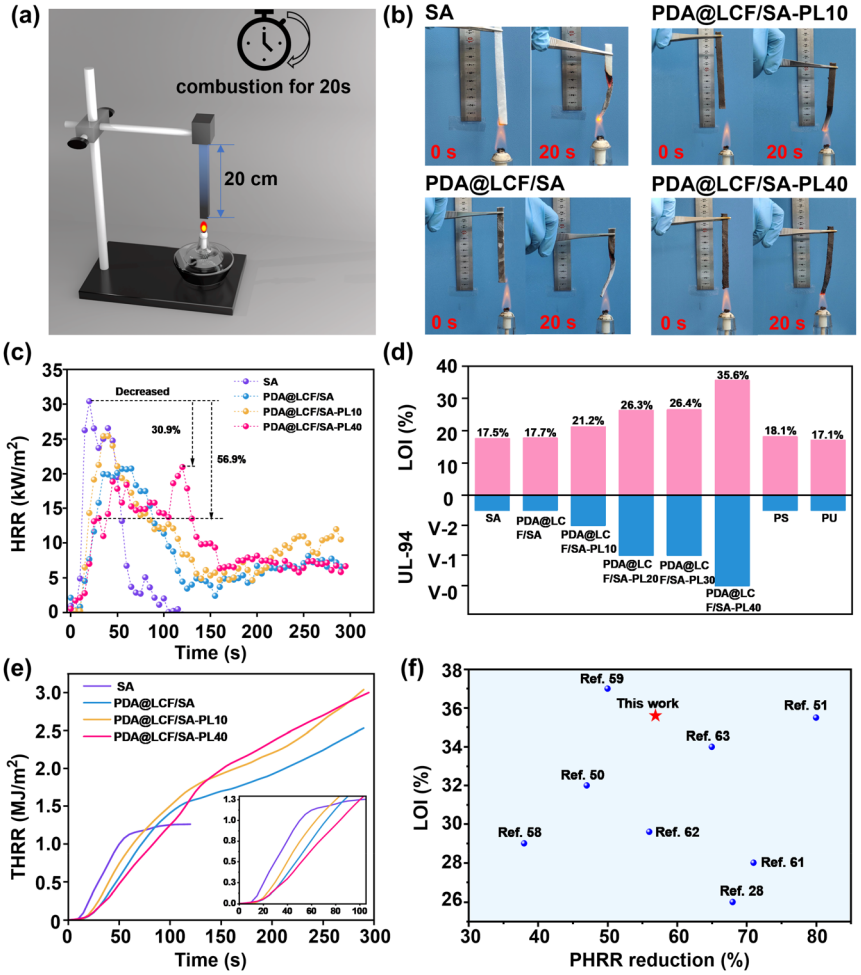

Fig. 4 (a and b) Vertical combustion test diagram for aerogel and presentation of vertical combustion test results. (c) HRR curves of different aerogel samples. (d) Summary of LOI values for different aerogel samples and commercial thermal insulation materials (PU and PS). (e) THR curves of different aerogel samples. (f) Comparison of LOI and PHRR reduction between the designed PDA@LCF/SA-PL40 and other existing lignin flame retardant aerogels.

The LOI, a critical parameter for evaluating flame retardant performance,[48] represents the minimum oxygen concentration (vol/vol%) required to sustain the combustion of a material for 3 min or consume a 5 cm length of the sample. This parameter was employed to assess the flame retardancy of the PDA@LCF-PLX composite aerogel. In this case, the SA and PDA@LCF composites exhibited lower LOI values of 17.5% and 17.7%, respectively (Fig. 4d). However, the LOI improved significantly upon incorporating phosphorylated lignin (PL) into the material matrix, with values increasing proportionally to the PL content. At a PL content of 40 wt%, the composite reached a maximum LOI of 35.6%. These results were consistent with the vertical UL-94 combustion tests, further confirming that PL served as an effective flame-retardant component within the material (Fig. S7 and Movie S4†).

A cone calorimeter was used to simulate real fire conditions and evaluate the heat release behavior of the composite aerogel at the combustion interface throughout the burning process.[49] Fig. 4c illustrates the heat release rate (HRR) curves for SA, PDA@LCF, and PDA@LCF-PL40 at a heat flux density of 35 kW m^{-2}. Comprehensive data are provided in Fig. 4e and Table 1. Specifically, the HRR curve of pure SA exhibited a rapid ascent to a peak value, followed by a slight decline, ultimately decreasing to a minimum and extinguishing within approximately 100 s. The PHRR values, identified as the first

Table 1 Cone calorimetric test data of different composite aerogel samples manufactured

Aerogel sample	P_1-HRR (kW m^{-2})	P_2-HRR (kW m^{-2})	T-HRR[a] (MJ m^{-2})	Char yield (%)
SA	30.3	26.6	20.1	4.5
PDA@LCF	25.5	N/A	21.2	3.6
PDA@LCF/SA-PL10	19.7	20.8	18.7	5.7
PDA@LCF/SA-PL40	13.6	21.1	16.6	10.6

[a] The THR test data displayed in the table were the data sampling of the first 120 s.

peak (P_1-HRR) and the second peak (P_2-HRR), were recorded at 30.3 kW m^{-2} and 26.6 kW m^{-2}, respectively. These findings indicated that pure SA possessed minimal flame-retardant capabilities and underwent a typical carbonization process during combustion. In contrast, although the HRR curve of PDA@LCF also demonstrated a significant rise, P_1-HRR exhibited merely a 16% decrease. This observation suggested that a singular nitrogen source additive was insufficient to significantly enhance the flame retardant performance. It was noteworthy that the parameters of PDA@LCF/PL10 exhibited slight decreases of 35.2% and 22.3%, respectively as compared to pure SA. However, as the lignin content increased to 40%, these parameters experienced significant reductions, with P_1-HRR and P_2-HRR being decreased by 56.9% and 30.9%, respectively. This phenomenon could be attributed to the demonstration of typical HRR characteristics associated with material combustion during the test. The formation of a protective carbon layer on the surface caused a gradual decline in HRR after the emergence of P_1-HRR, until volatile substances escaped through cracks in the carbon layer, leading to the emergence of P_2-HRR. Notably, the presence of PL was instrumental in delaying the onset of P_2-HRR. This phenomenon was attributed to the intrinsic structure of lignin, characterized by multiple benzene ring structures, as well as the synergistic interaction between the introduced phosphate groups and the nitrogen source in PDA@LCF. These factors collectively enhanced the charring ability of the material during combustion, thereby improving its flame-retardant properties. To assess the flame-retardant efficacy of PL composite aerogels, their performance was compared with previous studies utilizing P/N flame-retardants and modified lignin as flame-retardant components, as shown in Fig. 4f and Table 2. Investigating the synergistic flame-retardant mechanism of PDA@LCF and PL was considered important. To achieve this, we characterized the microscopic morphology of the residual carbon in all aerogels using scanning electron microscopy (SEM) and subsequently analysed the flame-retardant effect of phosphorus–nitrogen (P–N) compounds in the condensed phase. Fig. 5a presents the SEM images of the materials at varying resolutions with detailed data provided in Fig. S8 and Table S3.† It was observed that the density of the residual carbon layer in PDA@LCF/SA was slightly higher in comparison with that of pure SA, yet numerous micropores remained. This indicates that the its carbonization capacity was not significantly enhanced, allowing pyrolyzed combustible molecules to escape into the gas phase. This escape contributed to energy release during combustion and promoted smoke formation, ultimately limiting improvements in flame-retardant performance. Notably, the carbonization ability improved with increasing PL content when PL was incorporated into the material matrix. In particular, the carbon layer became denser when the PL content increased to 40%, and the pores were almost invisible, which effectively acted as a barrier against heat and smoke release. Furthermore, to more accurately define the degree of graphitization in SA and PDA@LCF/SA-PL40, we characterized the two samples using Raman spectroscopy (Fig. 5b). Notably, the Raman spectra of all tested samples exhibited overlapping peaks with intensity maxima at approximately 1590 and 1380 cm^{-1}. The peak at 1590 cm^{-1} corresponds to the G band, which are associated with the stretching vibration of the E2g symmetry in sp2 hybridized carbon atoms in graphite. In contrast, the peak at 1380 cm^{-1} represents the D band, indicative of sp3 defects in carbon, such as disordered graphite or glassy carbon. More importantly, the relative ratio of the integrated intensities of the D-band and G-band (I_D/I_G) were found to be inversely proportional to the in-plane crystallite size, where lower I_D/I_G values indicated the formation of more graphene-like structures during fire events.[50–52] Specifically, the I_D/I_G value of pure SA were 3.54, which decreased to 3.14 for PDA@LCF/SA-PL40. This decrease in I_D/I_G values suggested that higher PL content promoted the generation of graphene-like structures during combustion, thereby effectively protecting the underlying layer from further combustion. The chemical composition of the condensed phase was further examined using X-ray photoelectron spectroscopy (XPS) (Fig. 5c–e). Analysis of the O1s spectrum revealed that, as compared to pure SA, the binding energy peaks for C=O and C–O in PDA@LCF/SA-PL40 shifted, and their peak intensi-

Table 2 Comparison of fire resistance of designed the flame-retardant PDA@LCF/SA-PL40 aerogel material with similar materials

Flame-retardant system	PHRR reduction (%)	LOI (%)	UL-94 rating	Methods	Ref.
PDA@LCF/SA-PL40	56	36	V-0	Synergistic FR	This work
PLA/lignin/APP	47	32	V-0		53
PLA/lignin/MCAPP/OMMT	80	35	V-0		54
TPZ/AL/APP	80		V-0 like		55
PUF/lignin/APP	—	30	—		56
PLA/urea-modified lignin/APP	75	34	V-0	N-lignin	57
PUF/P-lignin	59	—	—	P-lignin	58
ABS/phosphorated lignin	58	—	—		59
EP/phosphorated lignin	43	—	V-1		60
GO/DOPO	38	29	V-0	Encapsulated	61
EG/APP/$CaCO_3$/EA	50	37	V-0		62
P(NTMS-POA)	68	26	V-0		63
N/P intumescent FR	71	28	V-1		64
HPCTP	56	29	V-0		65
PLA/Lig–Si/APP	65	34	V-0	Si-lignin	66

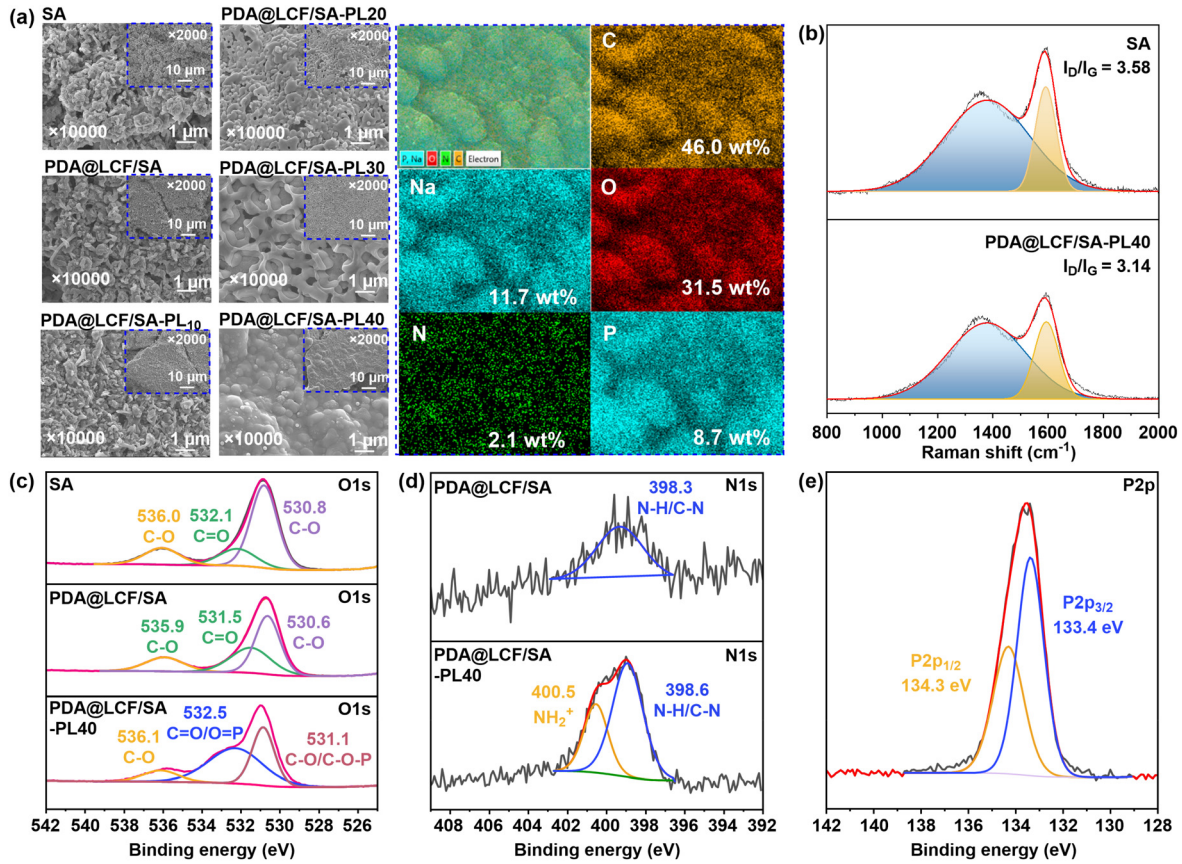

Fig. 5 Structural characterization and analysis of the aerogel. (a) SEM and mapping images of different samples after vertical combustion. (b) Raman spectra of pure SA and PDA@LCF/PL-40. (c) O1s XPS spectra of pure SA, PDA@LCF and PDA@LCF/SA-PL40. (d) N1s XPS spectra of PDA@LCF and PDA@LCF/SA-PL40. (e) P2p XPS spectra of PDA@LCF/SA-PL40.

ties were significantly enhanced (Fig. 5c). This enhancement was attributed to the formation of P═O and P–O–C covalent bond structures in PDA@LCF/SA-PL40 during the combustion process, which promoted cross-linking within the carbon layer and increased its densification.[67] It was noteworthy that the binding energy peaks corresponding to the C–N/N–H and NH_2^+ structures were observed in the N1s spectrum at 398.9 eV and 400.5 eV, respectively (Fig. 5d).[68] This observation was attributed to the activation of dopamine by phosphate within the system during combustion, which promoted the formation of a C–N structure in the condensed phase, and resulted in enhanced integrity of the carbon layer to mitigate heat transfer and the penetration of combustible gases. Meanwhile, a peak corresponding to P–N was observed at 133.4 eV, and a peak corresponding to P–O–C was observed at 134.3 eV (Fig. 5e).[69] This result further illustrated the synergistic effect of the nitrogen-containing groups in PDA and the phosphate groups in PL during the combustion process.

Thermogravimetric analysis-infrared spectroscopy (TG-IR) was employed to identify the gaseous pyrolysis products, thereby enhancing the understanding of the gas-phase flame retardant mechanism of the material (Fig. 6). Notably, SA exhibited a pronounced absorption peak at a lower temperature (Fig. 6a), which aligned with the TG results (Fig. S5†). In contrast, PDA@LCF/SA-PL40 displayed a diminished absorption peak (Fig. 6b). Specifically, pure SA released only a small amount of gaseous H_2O across various temperatures, whereas PDA@LCF/SA-PL40 released a greater quantity of gaseous H_2O as the temperature increased. This phenomenon was attributed to the release of H_2O resulting from the thermal degradation and condensation of cellulosic polysaccharides within the system. The rapid evaporation of water, an endothermic process, effectively reduced the temperature in the flame zone, thereby inhibiting the thermal degradation rate of the composite material. This was attributed to the involvement of the nitrogen element in the PDA coating. However, pure SA reached its peak CO_2 signal intensity at 457 °C, while PDA@LCF/SA-PL40 began to peak at 800 °C with its peak CO_2 intensity being lower than that of the former. This difference was ascribed to the introduction of PL, in which the phosphoric acid component was activated under high-temperature conditions, leading to the production of PO$^\bullet$ that captured OH$^\bullet$, H$^\bullet$, and other species involved in the combustion chain reaction. Additionally, the C–H absorption peaks observed between 2978 cm^{-1} and 2821 cm^{-1} along with the C–O–C absorption peak at 1065 cm^{-1}, typically associated with com-

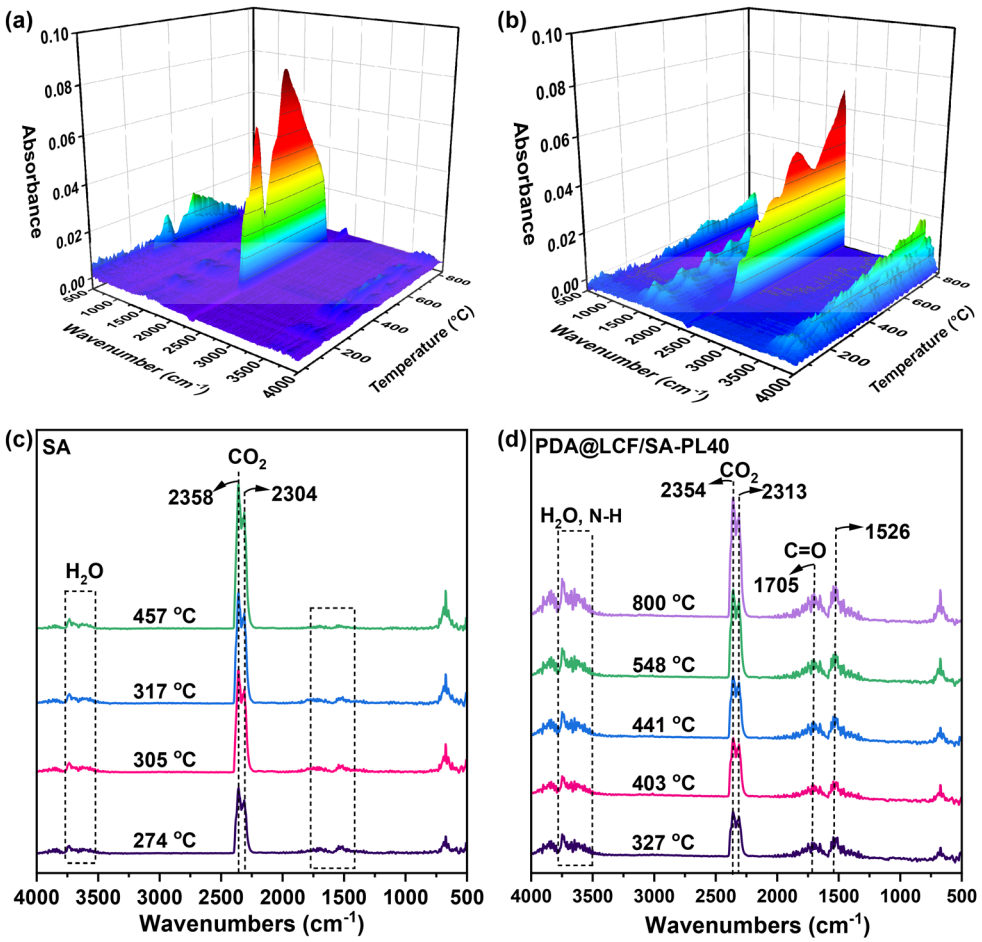

Fig. 6 Thermal degradation characterization and analysis of the aerogel. 3D TG-IR spectra for (a) pure SA, and (b) PDA@LCF/SA-PL40. FTIR spectra of volatiles produced from (c) Pure SA, and (d) PDA@LCF/SA-PL40 at different temperatures, respectively.

bustible substances such as alkanes and ethers, are absent in Fig. 6d. Instead, a new absorption band emerged at approximately 1705 cm^{-1} and 1500 cm^{-1}, likely arising from certain aromatic carbonyl compounds.[70] In the condensed phase, the macromolecular chain fragments of the material were dehydrated and cyclized in the presence of phosphoric acid. Simultaneously, the oxidative cross-linking of the PDA fragments, facilitated by phosphoric acid, enhanced the quality of the carbon layer. This carbon layer effectively obstructed heat and mass transfer as well as oxygen penetration, ultimately achieving a synergistic flame-retardant effect.

Based on the comprehensive analysis presented above, potential flame-retardant mechanisms for the designed PDA@LCF/SA-PL40 are proposed (Fig. 7). Upon exposure to heat, the synergistic interaction between the phosphate groups in PL within the aerogel and the PDA coating of LCF facilitated the dehydration of the material, resulting in the formation of a dense carbon layer. This phenomenon resulted from the dehydration reactions of hydroxyl, phosphate, and catechol groups within the system at elevated temperatures, leading to the formation of a stable cross-linked network. As the temperature was further increased, the breakdown of chemical bonds in the aerogel matrix resulted in the release of volatile substances, primarily non-flammable gases, such as water vapor, CO_2, and N_2. These contributed to the dilution of combustible gases and oxygen concentrations. As combustion progressed, phosphoric acid groups at the combustion interface were activated, releasing $PO^{\bullet}$ radicals. These radicals effectively captured $O^{\bullet}$ and $HO^{\bullet}$ radicals, disrupting the chain reaction and suppressing flame propagation. In the condensed phase, the macromolecular chain fragments of the material underwent dehydration and cyclization in the presence of phosphoric acid. Simultaneously, the oxidative cross-linking of the PDA@LCF fragments, facilitated by phosphoric acid, enhanced the quality of the carbon layer. This carbon layer effectively blocked heat and mass transfer as well as oxygen penetration, ultimately achieving a synergistic flame-retardant effect.

2.4 Hydrophobic and UV protection performance

Environmental factors were identified as significant influences on the durability of insulation materials, including ultraviolet radiation and rain erosion.[71] It has been demonstrated that enhancing the UV resistance and hydrophobic properties of thermal insulation materials effectively extended their service

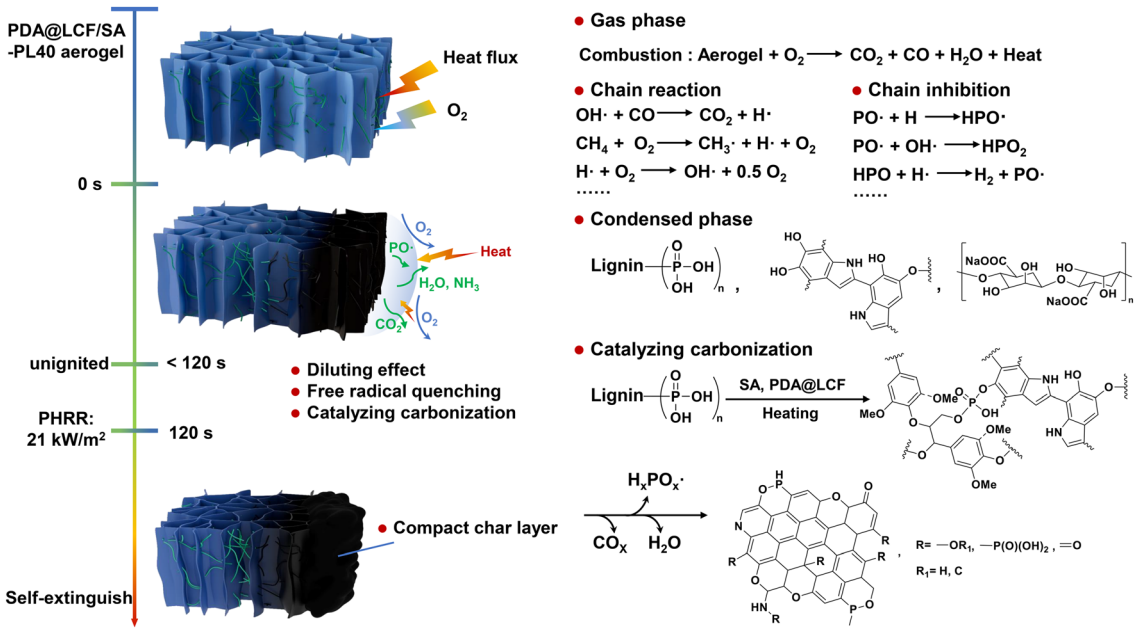

Fig. 7 Schematic of the proposed flame retardancy mechanism.

life, thereby improving economic benefits. Furthermore, the incorporation of eco-friendly additives to enhance the specialized properties of materials has gained widespread support. For this reason, lignin was utilized as one of the external additives due to its exceptional intrinsic UV absorption capacity and effective free radical scavenging ability, thereby enhancing the flame-retardant properties and improving its UV protective performance. Simultaneously, a simple vapor deposition method was utilized to construct a hydrophobic coating on the surface of the material, thereby improving its overall performance. The results indicated that the UPF value of the material reached as high when the PL content was 40 wt%, while the average transmittance of the material was measured at 0.05% in both the UVA and UVB bands (Table S3†). Simultaneously,

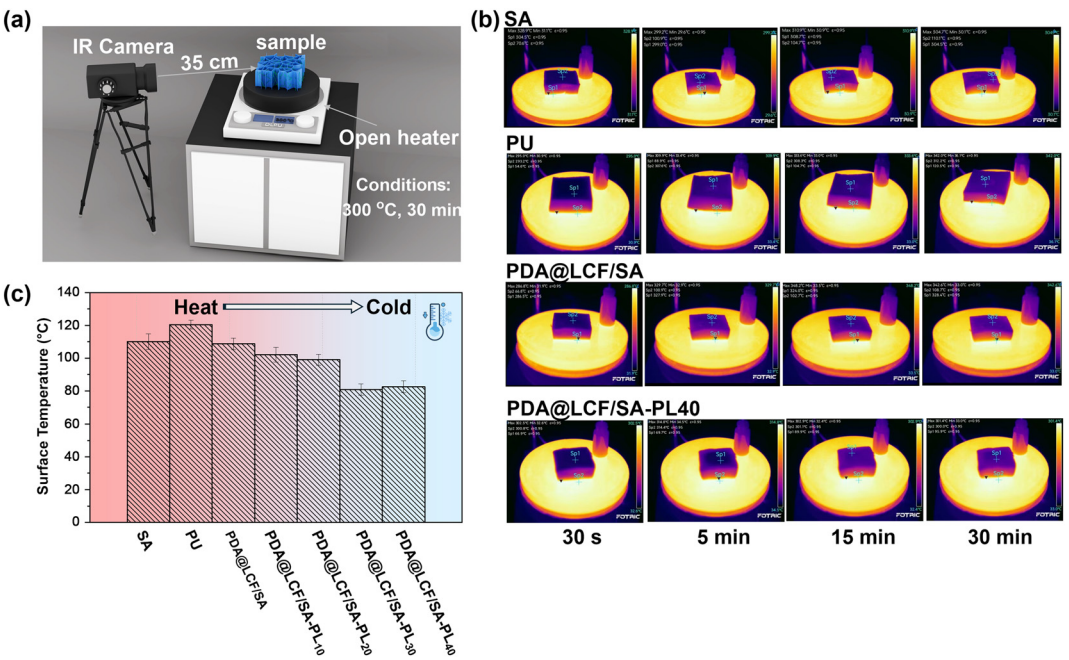

Fig. 8 Characterization and analysis of thermal insulation properties of the composite aerogel. (a) Schematic diagram of a homemade device used to evaluate insulation performance. (b) Infrared photos of different aerogels and commercial thermal insulation materials (PU). (c) Summary of the surface temperature of different materials after heating for 30 min.

static dripping experiments were conducted using methyl blue and methyl orange to assess the water resistance of the material (Fig. S9a†). It was evident that the surface tension of pure SA was low, resulting in easy wetting by droplets. In contrast, the PDA@LCF/SA-PL40 sample, which featured a hydrophobic coating, exhibited no wetting when the droplets fell. This observation aligned with the results from the water contact angle test (Fig. S9b†).

2.5 Excellent thermal insulation

Building insulation materials require not only excellent flame-retardant properties, but also effective thermal insulation.[72] To demonstrate the potential application of the composite aerogel as a thermal insulation material, the actual thermal insulation properties of various samples were compared with those of other common thermal insulation materials, such as polystyrene (PS) and polyurethane (PU). A thermal infrared imaging device was used to monitor the variation in the surface temperature of samples placed on a 300 °C hot plate over a duration of 30 min (Fig. 8a and b). All samples were measured 5 cm × 5 cm × 2 cm. Specifically, pure SA rapidly heated to approximately 100 °C within 5 min, followed by a gradual increase that ultimately reached about 110 °C after 30 min. Meanwhile, the surface temperature of commercial PU was approximately 3 °C lower than that of pure SA at the 30 min mark. It was noteworthy that the volume of PS underwent significant shrinkage within 5 min of heating, indicating that its operating temperature was substantially lower than 300 °C (Fig. 8b). The addition of PL enhanced its thermal insulation properties to some extent. Furthermore, as the PL content increased, the thermal insulation performance improved with an optimal PL content of 40 wt%. Comparatively, the temperature remained below 90 °C after 15 min of heating and reached 95 °C after 30 min (Fig. 8b and c). This observation demonstrated that a higher PL content could effectively enhance the thermal insulation performance of the aerogel.

3. Conclusions

In summary, we report a novel solvent-free mechanochemical method to generate PL. Concurrently, PDA@LCF was incorporated into the system to establish a P–N based flame-retardant system with PL, leading to the development of thermal insulation aerogels exhibiting exceptional flame-retardant properties. Notably, the prepared lignin composite aerogels were nearly non-combustible, demonstrating a 56.9% reduction in P_1HRR, a 39.6% reduction in P_2HRR, and an LOI as high as 35.6%. Furthermore, the aerogels successfully passed the UL-94 flammability test, achieving a V-0 rating. Due to the synergistic interaction between PDA@LCF and lignin phosphide, the condensed phase formed a solid carbon layer with a complete structure that acted as a fire barrier. Additionally, the phosphoric acid component of lignin exhibited a strong free radical scavenging effect, effectively capturing burning free radicals at the combustion interface and achieving a synergistic flame-retardant effect. Additionally, the fabricated aerogel revealed excellent thermal insulation properties, making it a viable alternative to traditional thermal insulation sheets. Overall, this work presented an innovative design concept for developing the next generation of fire insulation materials, facilitating advancements in this field and offering broad application prospects in construction and commercial insulation.

4. Experimental

4.1 Pretreatment of lignin and phosphating modification of lignin

First, 20 g of pre-hydrolyzed lignin was dissolved in 1,4-dioxane solution and stirred for 4 h. Next, the volume of the lignin mixed solution was concentrated to 1/3 of the original volume using a rotary evaporator. The obtained lignin concentrate was added dropwise to acid water with pH = 2 and allowed to stand in a refrigerator at 4 °C for 24 h. The supernatant was then removed by vacuum filtration and continuously rinsed with deionized water. The obtained precipitate was freeze-dried to obtain the purified pre-hydrolyzed lignin (L).

The steps of lignin modification were carried out according to previous literature with slight modifications.[73] Typically, 3.0 g of lignin, 6.0 g of P_2O_5, and 1.0 g of urea were mixed in a 250 mL zirconia jar and ground at 250 rpm for 8 h using a zirconia ball with a diameter of 10 mm. Then, the obtained sample was evenly dispersed in deionized water. Afterwards, the mixed solution was purified using a dialysis tube with a molecular weight cutoff of 1000 Da. Finally, phosphorylated lignin (PL) was obtained by lyophilization.

4.2 Pretreatment of softwood fiber pulp and fabrication of dopamine-modified lignocellulose (PDA@LCF)

First, the softwood pulp board was mechanically dispersed to obtain fiber slurry, and then the wet fibers were filtered and stored in a refrigerator at 4 °C. Next, a more dispersed fiber is obtained by means of simple mechanical ball milling. Specifically, the dispersed 6.0 g lignocellulose was packed in a 250 mL zirconia tank, and a zirconia ball with a diameter of 10 mm was ground for 2 h at 400 rpm. Finally, the obtained lignocellulose (LCF) was pretreated.

The dopamine modification of lignocellulose was carried out through a typical step with modified cellulose. Typically, 0.4 g Tris was dissolved in 100 mL water and gradually added to 0.1 mol L^{-1} HCl solution until the pH reached 8.5. Then 0.4 g of dopamine hydrochloride was added to get the PDA precursor solution. LCF was then immersed in the solution for 48 h to obtain the lignocellulose surface loaded with polydopamine (PDA@LCF).

4.3 Preparation of lignin composite aerogel: the lignin composite

Aerogel composition is shown in Fig. 3a. For example, to fabricate lignin composite aerogel, 4.0 g PL and 2.0 g PDA@LCF

were uniformly dispersed in an aqueous solution with pH 12. Then, 4.0 g SA was added and stirred at 200 rpm for 4 h. After that, it was introduced into a special mold and unidirectional freezing with liquid nitrogen. Subsequently, the monoliths were lyophilized at −40 °C under 0.1 Pa for 3 days to obtain the lignin composite aerogel. The final product was named SA/PDA@LCF-PL40, of which SA represents sodium alginate, PDA@LCF represents dopamine-modified lignocellulose, PL represents phosphorylated lignin, and the subscripts represent PL contents. The other samples were prepared by the same method.

Author contributions

Tao Gui: original draft, visualization, validation, methodology, investigation, and data curation. Shuang-Lin Zou: validation. Hao-Zhen Dou: validation. Wen-Feng Ren: validation. Chang-You shao: validation. Chun-Lin Xu: validation. Ling-Ping Xiao: writing – review & editing, writing – original draft, supervision, resources, project administration, funding acquisition, and conceptualization. Run-Cang Sun: writing – review & editing and project administration.

Data availability

The data used to support the findings of this study are available from the corresponding author upon request.

Conflicts of interest

The authors declare that they have no known competing financial interests or personal relationships that could have appeared to influence the work reported in this paper.

Acknowledgements

This work was supported by the National Natural Science Foundation of China (22278049, U24A20559, and 22478046), the Dalian High-Level Talent Innovation Program (2024RJ017), and the Energy Revolution S&T Program of Yulin Innovation Institute of Clean Energy (YIICEE411060316).

References

1 S. B. Sadineni, S. Madala and R. F. Boehm, *Renewable Sustainable Energy Rev.*, 2011, **15**, 3617–3631.
2 M. Cao, B.-W. Liu, L. Zhang, Z.-C. Peng, Y.-Y. Zhang, H. Wang, H.-B. Zhao and Y.-Z. Wang, *Compos. Part B-Eng.*, 2021, **225**, 109309.
3 M. Raza, H. Al Abdallah, M. Kozal, A. Al Khaldi, T. Ammar and B. Abu-Jdayil, *J. Build. Eng.*, 2023, **75**, 106982.
4 X. Zhang, J. Zhao, K. Liu, G. Li, D. Zhao, Z. Zhang, J. Wan, X. Yang, R. Bai and Y. Wang, *Natl. Sci. Rev.*, 2022, **9**, nwac012.
5 L. Lujan, M. a. L. Goñi and R. E. Martini, *ACS Sustainable Chem. Eng.*, 2022, **10**, 12000–12008.
6 A. Dixit, S. D. Pang, S.-H. Kang and J. Moon, *Cem. Concr. Compos.*, 2019, **102**, 185–197.
7 J. P. Cárdenas-R, M. Cea, K. Santín, G. Valdés, R. Hunter and R. Navia, *Compos. Part B-Eng.*, 2018, **132**, 10–16.
8 J. Sun, Z. Wu, B. An, C. Ma, L. Xu, Z. Zhang, S. Luo, W. Li and S. Liu, *Compos. Part B-Eng.*, 2021, **220**, 108997.
9 Q. Lv, X. Zhu, T. Zhou, L. Tian, Y. Liu, Y. Wang and C. Zhang, *Constr. Build. Mater.*, 2024, **423**, 135902.
10 M. Oschatz, L. Borchardt, K. Pinkert, S. Thieme, M. R. Lohe, C. Hoffmann, M. Benusch, F. M. Wisser, C. Ziegler, L. Giebeler, M. H. Rümmeli, J. Eckert, A. Eychmüller and S. Kaskel, *Adv. Funct. Mater.*, 2014, **4**, 1300645.
11 Y. Zhuo, J. He, W. Li, J. Deng and Q. Lin, *Environ. Pollut.*, 2023, **337**, 122518.
12 S. Yang, Y. Li, M. Nie, X. Liu, Q. Wang, N. Chen and C. Zhang, *Adv. Mater.*, 2024, **36**, 2404115.
13 S. Wang, R. Ding, G. Liang, W. Zhang, F. Yang, Y. Tian, J. Yu, S. Zhang and B. Ding, *Adv. Mater.*, 2024, **36**, 2313444.
14 T. Wang, M.-C. Long, H.-B. Zhao, B.-W. Liu, H.-G. Shi, W.-L. An, S.-L. Li, S.-M. Xu and Y.-Z. Wang, *J. Mater. Chem. A*, 2020, **8**, 18698–18706.
15 T. Liu, T. Liu, H. Huang, J. Yu, Z. Hu and Y. Wang, *Chem. Eng. J.*, 2024, **497**, 154590.
16 X. Liang, Q. Sun, X. Zhang, Z. Hu, M. Liu, P. Gu, X. Yang and G. Zu, *Adv. Funct. Mater.*, 2024, **34**, 2408707.
17 M. Häußler, M. Eck, D. Rothauer and S. Mecking, *Nature*, 2021, **590**, 423–427.
18 C. Wang, F. Eisenreich and Ž. Tomović, *Adv. Funct. Mater.*, 2024, 2314447.
19 S. Wang, N. Wang, D. Kai, B. Li, J. Wu, J. C. C. Yeo, X. Xu, J. Zhu, X. J. Loh and N. Hadjichristidis, *Nat. Commun.*, 2023, **14**, 1182.
20 L. Zhang, Y. Liao, Y.-C. Wang, S. Zhang, W. Yang, X. Pan and Z. L. Wang, *Adv. Funct. Mater.*, 2020, **30**, 2001763.
21 A. Varamesh, Y. Zhu, G. Hu, H. Wang, H. Rezania, Y. Li, Q. Lu, X. Ren, F. Jiang and S. L. Bryant, *Chem. Eng. J.*, 2024, **495**, 153587.
22 K. Yang, Y. Zhou, Z. Wang, M. Li, D. Shi, X. Wang, T. Jiang, Q. Zhang, B. Ding and J. You, *Adv. Mater.*, 2021, **33**, 2007596.
23 J. Zhou, R. Zhang, R. Xu, Y. Li, W. Tian, M. Gao, M. Wang, D. Li, X. Liang, L. Xie, K. Liang, P. Chen and B. Kong, *Adv. Funct. Mater.*, 2022, **32**, 2111406.
24 B. Thomas, M. C. Raj, J. Joy, A. Moores, G. L. Drisko and C. Sanchez, *Chem. Rev.*, 2018, **118**, 11575–11625.
25 L. Li, R. Wang, Y. Fu, Z. Jin, J. Chen, H. Du, X. Pan and Y.-C. Wang, *Adv. Funct. Mater.*, 2024, **35**, 2412324.
26 S. Tang, M. Ma, X. Zhang, X. Zhao, J. Fan, P. Zhu, K. Shi and J. Zhou, *Adv. Funct. Mater.*, 2022, **32**, 2205417.
27 C. Senthil, S.-S. Kim and H. Y. Jung, *Nat. Commun.*, 2022, **13**, 145.

28 S. T. Lazar, T. J. Kolibaba and J. C. Grunlan, *Nat. Rev. Mater.*, 2020, **5**, 259–275.
29 M. S. Webber, J. Watson, J. Zhu, J. H. Jang, M. Çağlayan, J. S. Heyne, G. T. Beckham and Y. Román-Leshkov, *Nat. Mater.*, 2024, **23**, 1622–1638.
30 J. Sternberg and S. Pilla, *Nat. Sustain.*, 2023, **6**, 316–324.
31 H.-Y. Ma, L.-F. Tong, Z.-B. Xu and Z.-P. Fang, *Adv. Funct. Mater.*, 2008, **18**, 414–421.
32 Y. Matsushita, D. Hirano, D. Aoki, S. Yagami, Y. Takagi and K. Fukushima, *Adv. Sustainable Syst.*, 2017, **1**, 1700073.
33 F. Yu, Z. Ba, Z. Gao, Y. Wang, Y. Xie, H. Wang, Z. Qiu and Z. Xiao, *Chem. Eng. J.*, 2024, **493**, 152827.
34 L. Liu, M. Qian, P. a. Song, G. Huang, Y. Yu and S. Fu, *ACS Sustainable Chem. Eng.*, 2016, **4**, 2422–2431.
35 L. Cao, H. Shan, D. Zong, X. Yu, X. Yin, Y. Si, J. Yu and B. Ding, *Nano Lett.*, 2022, **22**, 1609–1617.
36 B.-W. Liu, H.-B. Zhao, L. Chen, L. Chen, X.-L. Wang and Y.-Z. Wang, *Composites, Part B*, 2021, **211**, 108664.
37 F. J. García-Mateos, R. Berenguer, M. J. Valero-Romero, J. Rodríguez-Mirasol and T. Cordero, *J. Mater. Chem. A*, 2018, **6**, 1219–1233.
38 Y. Guo, A. Baschieri, F. Mollica, L. Valgimigli, J. Cedrowski, G. Litwinienko and R. Amorati, *Angew. Chem., Int. Ed.*, 2021, **60**, 15220–15224.
39 Y. Hou, G. Zhu, S. O. Catt, Y. Yin, J. Xu, E. Blasco and N. Zhao, *Adv. Sci.*, 2023, **10**, 2304147.
40 B.-W. Liu, H.-B. Zhao and Y.-Z. Wang, *Adv. Mater.*, 2022, **34**, 2107905.
41 J. Liu, X. Cui, Y. Qu, X. Su, X. Li, P. Qi, H. Li, X. Gu, J. Sun and S. Zhang, *ACS Sustainable Chem. Eng.*, 2024, **12**, 12670–12682.
42 X. Guo, Y. Ma, Z. Li, Q. Jiang, Z. Jiang and B. Shi, *Chem. Eng. J.*, 2023, **478**, 147362.
43 Y. Tan, Z.-B. Shao, L.-X. Yu, J.-W. Long, M. Qi, L. Chen and Y.-Z. Wang, *Polym. Chem.*, 2016, **7**, 3003–3012.
44 T. Chaudhari, N. Rajagopalan and K. Dam-Johansen, *ACS Sustainable Chem. Eng.*, 2024, **12**, 7813–7830.
45 B. Prieur, M. Meub, M. Wittemann, R. Klein, S. Bellayer, G. Fontaine and S. Bourbigot, *RSC Adv.*, 2017, **7**, 16866–16877.
46 M. Liu, J. Qiao, X. Zhang, Z. Guo, X. Liu, F. Lin, M. Yang, J. Fan, X. Wu and Z. Huang, *Adv. Funct. Mater.*, 2024, **35**, 2412492.
47 D. Kumar, M. Alam, P. X. Zou, J. G. Sanjayan and R. A. Memon, *Renewable Sustainable Energy Rev.*, 2020, **131**, 110038.
48 Z. X. Zhang, J. Zhang, B.-X. Lu, Z. X. Xin, C. K. Kang and J. K. Kim, *Compos. Part B-Eng.*, 2012, **43**, 150–158.
49 K.-C. Tsai, *J. Hazard. Mater.*, 2009, **172**, 763–772.
50 C. Reti, M. Casetta, S. Duquesne, S. Bourbigot and R. Delobel, *Polym. Adv. Technol.*, 2008, **19**, 628–635.
51 R. Zhang, X. Xiao, Q. Tai, H. Huang, J. Yang and Y. Hu, *J. Appl. Polym. Sci.*, 2013, **127**, 4967–4973.
52 L. Verdolotti, M. Oliviero, M. Lavorgna, S. Iannace, G. Camino, P. Vollaro and A. Frache, *Polym. Degrad. Stab.*, 2016, **134**, 115–125.
53 W. Lu, Q. Li, Y. Zhang, H. Yu, S. Hirose, H. Hatakeyama, Y. Matsumoto and Z. Jin, *J. Wood Sci.*, 2018, **64**, 287–293.
54 R. Zhang, X. Xiao, Q. Tai, H. Huang and Y. Hu, *Polym. Eng. Sci.*, 2012, **52**, 2620–2626.
55 W. Xing, H. Yuan, P. Zhang, H. Yang, L. Song and Y. Hu, *J. Polym. Res.*, 2013, **20**, 1–12.
56 B. Prieur, M. Meub, M. Wittemann, R. Klein, S. Bellayer, G. Fontaine and S. Bourbigot, *Polym. Degrad. Stab.*, 2016, **127**, 32–43.
57 G. P. Mendis, S. G. Weiss, M. Korey, C. R. Boardman, M. Dietenberger, J. P. Youngblood and J. A. Howarter, *Green Mater.*, 2016, **4**, 150–159.
58 L. Li, X. Shao, Z. Zhao, X. Liu, L. Jiang, K. Huang and S. Zhao, *ACS Omega*, 2020, **5**, 799–807.
59 K. Li, Y. Li, Y. Zou, B. Yuan, A. Walsh and D. Carradine, *Fire Technol.*, 2023, **59**, 29–51.
60 Z.-M. Zhu, Y.-J. Xu, W. Liao, S. Xu and Y.-Z. Wang, *Ind. Eng. Chem. Res.*, 2017, **56**, 4649–4658.
61 G. Wang, X. Chen, P. Liu and S. Bai, *J. Appl. Polym. Sci.*, 2017, **134**, 44356.
62 G. Wang, W. Li, S. Bai and Q. Wang, *ACS Omega*, 2019, **4**, 9306–9315.
63 R. Zhang, X. Xiao, Q. Tai, H. Huang, J. Yang and Y. Hu, *High Perform. Polym.*, 2012, **24**, 738–746.
64 K. Avinash and F. Patolsky, *Mater. Today*, 2023, **70**, 104–136.
65 A. Sadezky, H. Muckenhuber, H. Grothe, R. Niessner and U. Pöschl, *Carbon*, 2005, **43**, 1731–1742.
66 H.-B. Zhao, B.-W. Liu, X.-L. Wang, L. Chen, X.-L. Wang and Y.-Z. Wang, *Polymer*, 2014, **55**, 2394–2403.
67 Y.-H. Guan, J.-Q. Huang, J.-C. Yang, Z.-B. Shao and Y.-Z. Wang, *Ind. Eng. Chem. Res.*, 2015, **54**, 3524–3531.
68 K. Chen, J. Liu, H. Bian, W. Wang, F. Wang and Z. Shao, *J. Electroanal. Chem.*, 2020, **878**, 114473.
69 S. Ran, F. Fang, Z. Guo, P. Song, Y. Cai, Z. Fang and H. Wang, *Compos. Part B-Eng.*, 2019, **170**, 41–50.
70 F. Song, C. Huang, X. Zhu, C. Liu, Y. Zhou and P. Jia, *J. Appl. Polym. Sci.*, 2021, **138**, 50809.
71 T. Rahman, A. N. Tajudin, F. Suwarto, P. Sudigdo and N. Thom, *Sustain. Cities Soc.*, 2024, **112**, 105625.
72 P. S. Jadhav, A. Sarkar, S. Pasupathy and S. Ren, *Adv. Eng. Mater.*, 2023, **25**, 2300037.
73 G.-J. Jiao, J. Ma, J. Hu, X. Wang and R. Sun, *J. Hazard. Mater.*, 2023, **448**, 130988.